Science Translational Medicine
AAAS

Supplementary Materials for

Engineered PLGA microparticles for long-term, pulsatile release of STING agonist for cancer immunotherapy

Xueguang Lu, Lei Miao, Wenting Gao, Ziqi Chen, Kevin J. McHugh, Yehui Sun, Zachary Tochka, Stephanie Tomasic, Kaitlyn Sadtler, Alain Hyacinthe, Yuxuan Huang, Tyler Graf, Quanyin Hu, Morteza Sarmadi, Robert Langer*, Daniel G. Anderson*, Ana Jaklenec*

*Corresponding author. Email: rlanger@mit.edu (R.L.); dgander@mit.edu (D.G.A.); jaklenec@mit.edu (A.J.)

The PDF file includes:

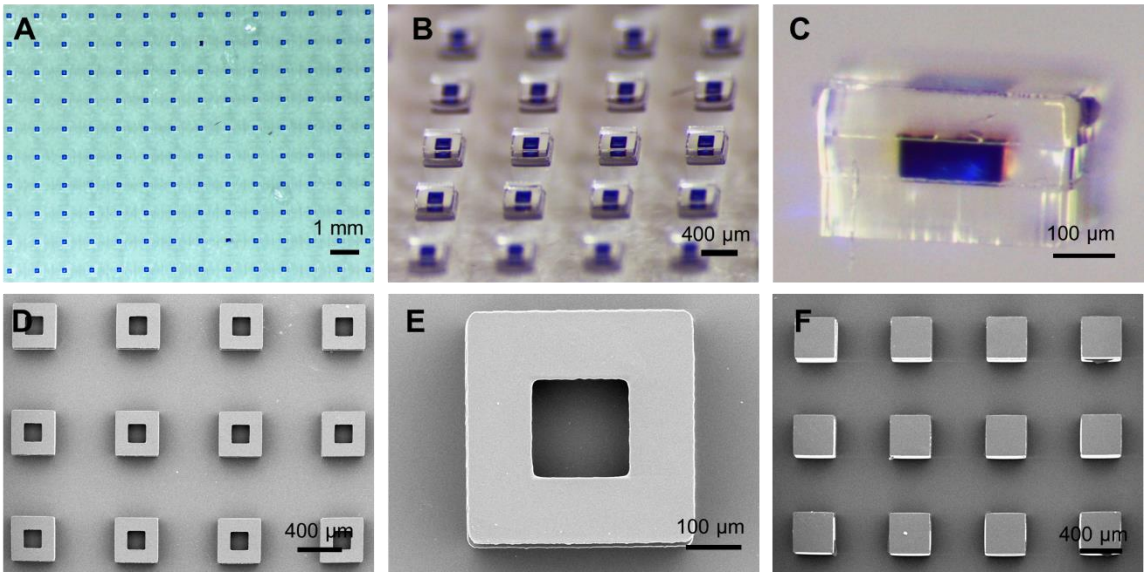

Fig. S1. Additional optical and scanning electron microscopy images of microparticles. Optical images of AF647-dextran filled bases (**A**) and sealed particles at low (**B**) and high magnifications (**C**). Scanning electron microscopy images of empty microparticle bases at low (**D**) and high magnifications (**E**), and sealed microparticles (**F**).

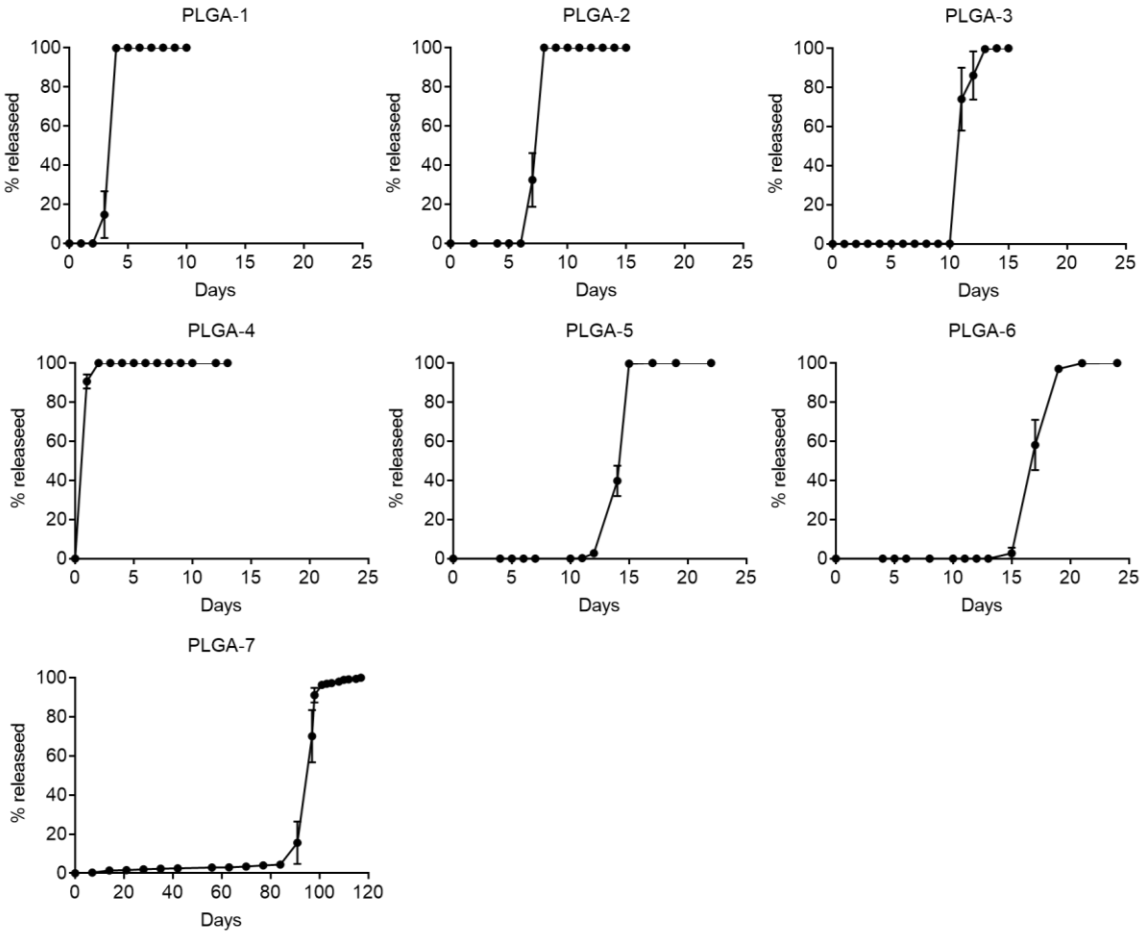

Fig. S2. Cumulative in vitro release kinetics of AF647-dextran from PLGA-MPs. Data are shown as mean ± SEM (n = 6 to 8).

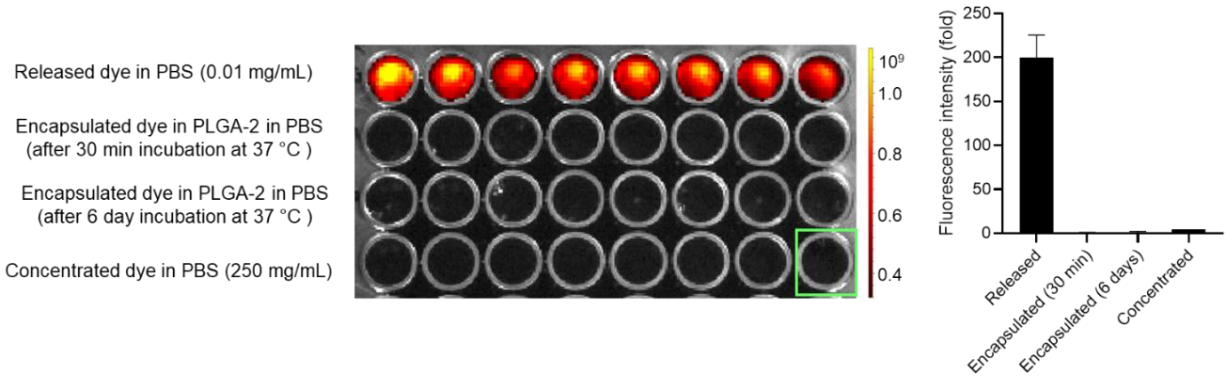

Fig. S3. Fluorescence of AF647-dextran was quenched before release from microparticles. PLGA microparticles encapsulating AF647-dextran were incubated in PBS at 37 °C for 30 min or for 6 days. Released AF647-dextran from PLGA-2 (after 8 days incubation at 37 °C) in PBS at 0.01 mg/mL was used as a positive control. A concentrated AF647-dextran solution of 250 mg/mL in PBS was used to mimic the dye concentration in the particle core. IVIS image (left) and corresponding quantitative (right) analysis showed that fluorescence intensity of released AF647-dextran is over 100-fold stronger than that of encapsulated AF647 in particles (n = 8 for released and encapsulated dye groups, n = 1 for concentrated dye in PBS). Data are shown as mean ± SD.

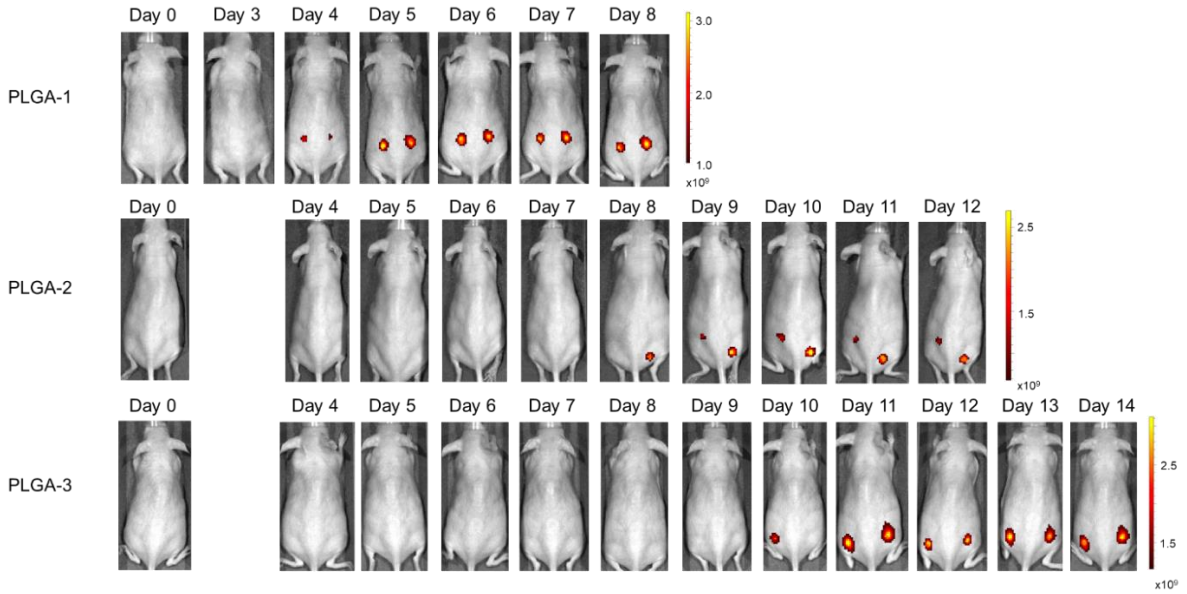

Fig. S4. Representative IVIS images of mice that received AF647-dextran–loaded PLGA-MPs. PLGA-MPs were subcutaneously injected into both the left and right flanks. Scale bars represent radiant efficiency.

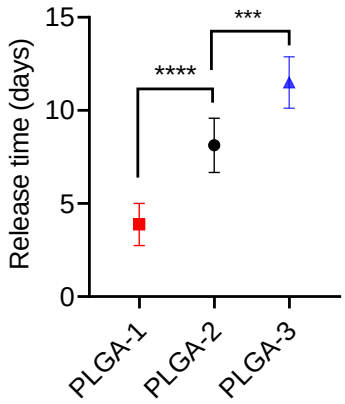

Fig. S5. Averaged release time of AF647-dextran from subcutaneously injected PLGA-MPs. Data are shown as mean ± SD (n = 6-8). Statistical significance was calculated by one-way analysis of variance (ANOVA). ***P < 0.001, ****P < 0.0001.

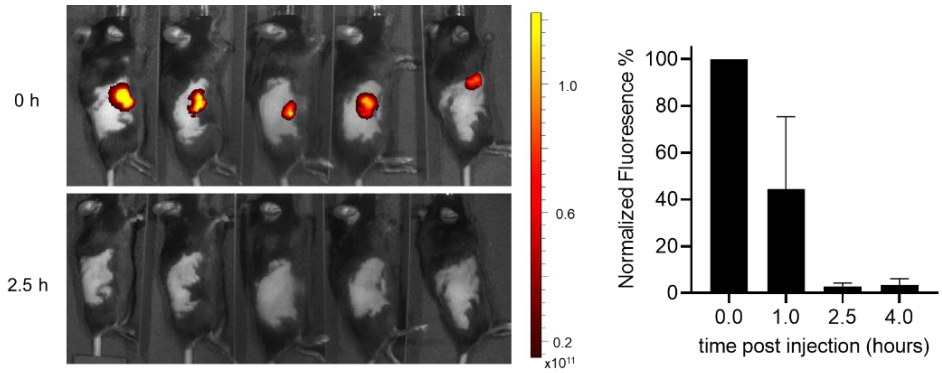

Fig. S6. Free AF647 was rapidly cleared from tumors. 5 μg of free AF647 in PBS buffer was intratumorally injected into mice with B16F10 tumors. The mice were imaged over time using an IVIS. IVIS image (left) and quantitative analysis (right) showed that over 95% of free AF647 was cleared from tumors within 2.5 hours. Data are shown as mean ± SD (n = 5).

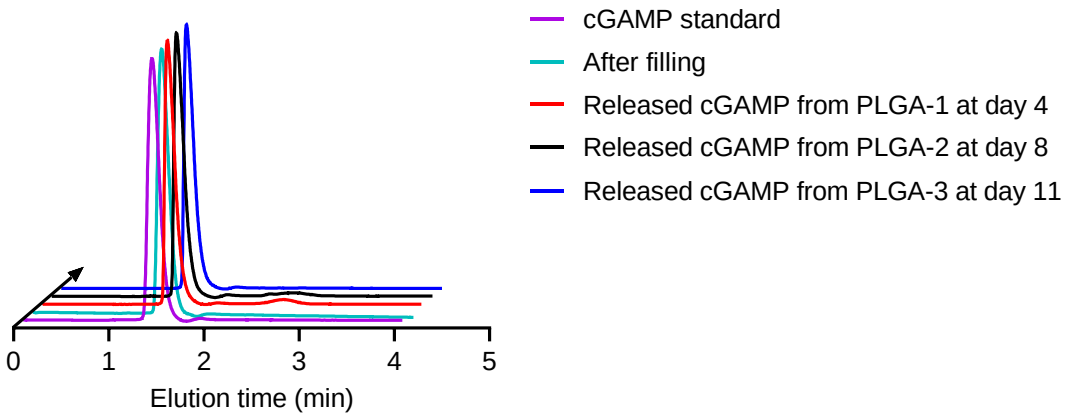

Fig. S7. HPLC analysis of cGAMP before and after release. HPLC chromatograms of 3'3'-cGAMP were prepared freshly, recovered after filling into PLGA microparticles, or following release from PLGA-1, 2, and 3 after 4, 8, and 11 days, respectively.

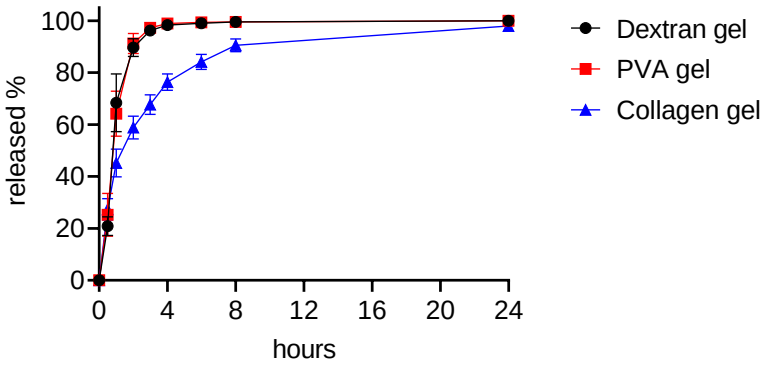

Fig. S8. Cumulative in vitro release of 3′3′-cGAMP from hydrogels. Data are shown as mean ± SD (n = 3-4).

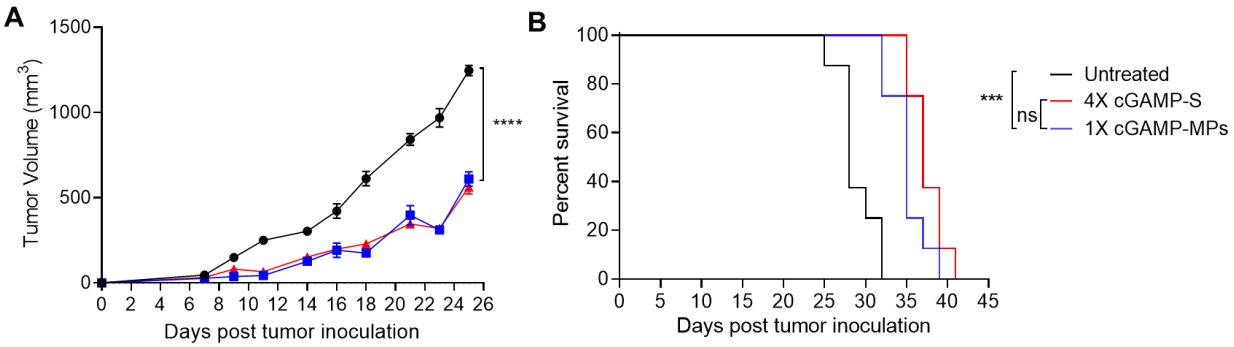

Fig. S9. Tumor growth and survival analysis of subcutaneous 4T1 breast tumor–bearing mice treated with cGAMP-MPs. Statistical significance was calculated by two-way ANOVA and Tukey's multiple comparisons test: ***P < 0.001, ****P < 0.0001. Data are shown as mean ± SEM (n = 8 biologically independent samples).

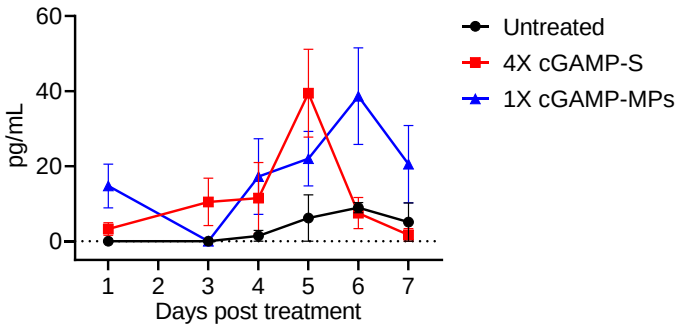

Fig. S10. Systemic IL-6 concentrations in orthotopic 4T1 tumor–bearing mice after treatments. The concentration of IL-6 in serum was evaluated by enzyme-linked immunosorbent assay (IL-6 mouse ELISA kit, Invivogen). Data are shown as mean ± SEM (n = 3).

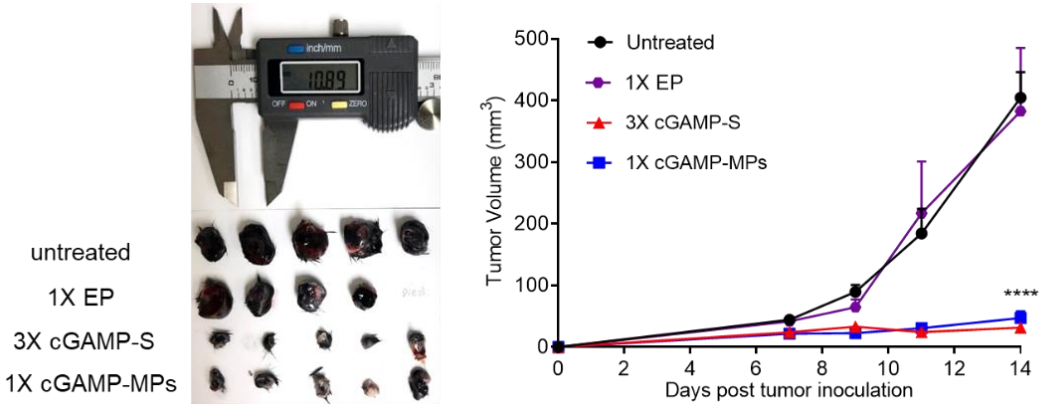

Fig. S11. Representative image of B16F10 tumors and average tumor growth curve after treatments. One of 1× EP treated mouse died before collecting the tumors. Data represent mean ± SEM. (n = 4 to 5, see Fig. 4A for treatment regimen). Statistical significance was calculated by one-way ANOVA. ****P < 0.0001.

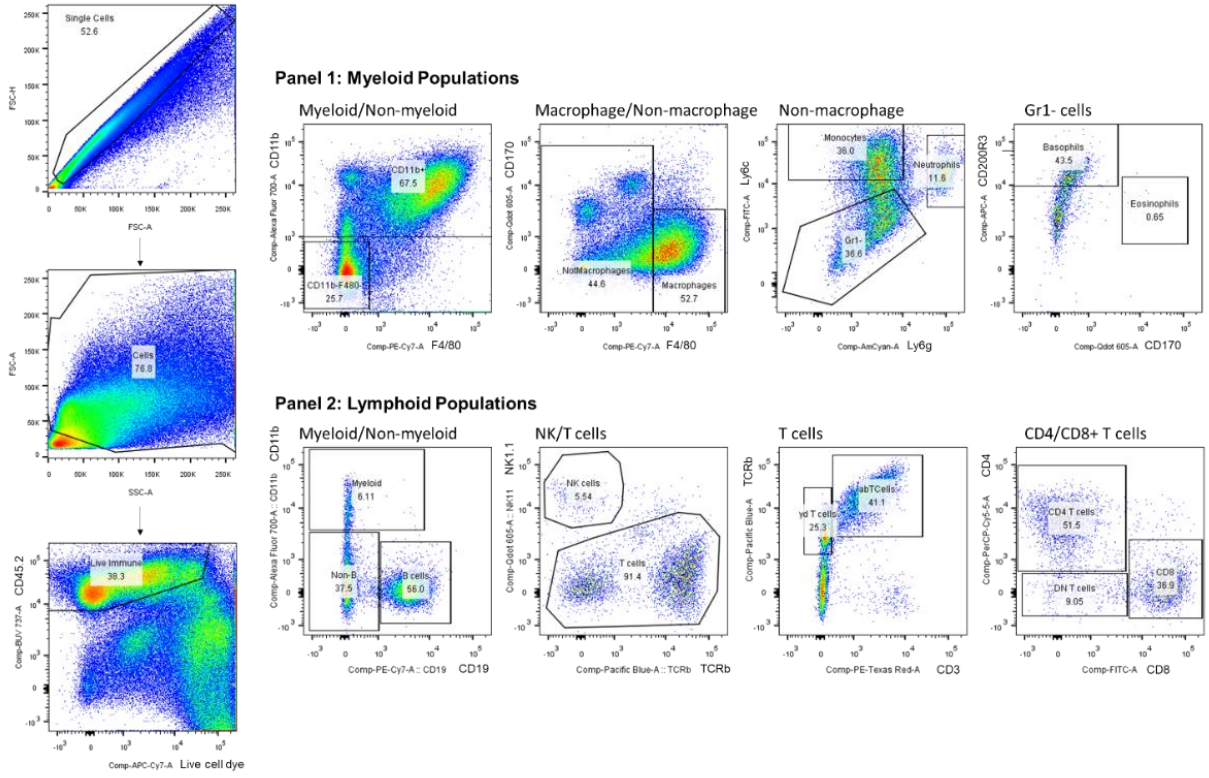

Fig. S12. Gating scheme for flow cytometry measurements of myeloid and lymphoid cells in TME.

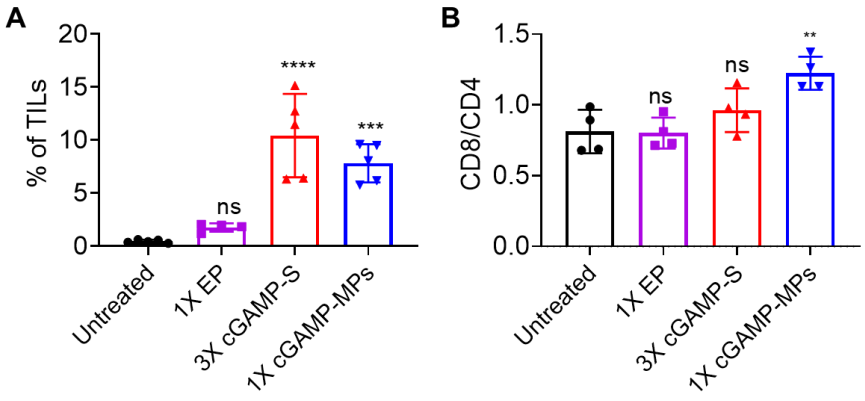

Fig. S13. Quantification of lymphocytes in the TME by flow cytometry. A. Percentages of tumor-infiltrating lymphocytes in different treatment groups (n = 4 or 5). **B.** Ratio of $CD8^+$ T cells and $CD4^+$T cells within TME (n = 4). Data are shown as mean **±** SD **, P < 0.01, ***, P < 0.001, ****, P < 0.0001, ns represents no significant difference, student's *t* test was used to compare with untreated group.

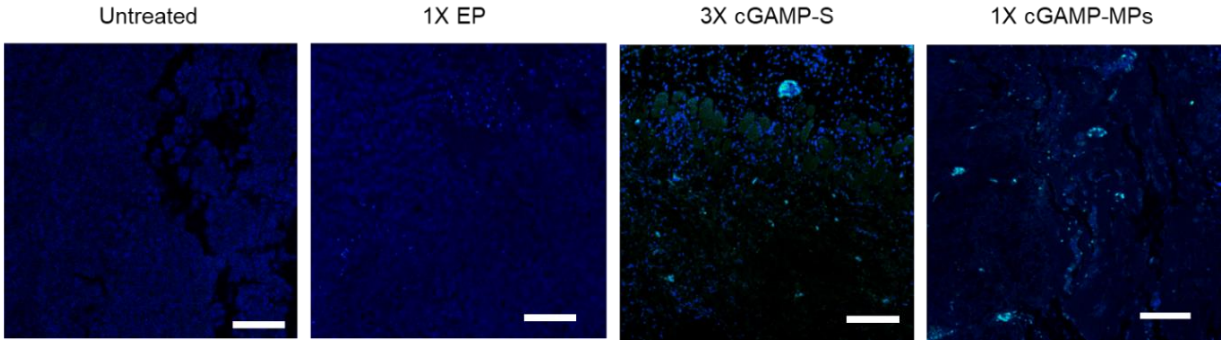

Fig. S14. Immunofluorescence images of histological sections of B16F10 tumors after treatments. Blue represents DAPI staining of nuclei. Green represents $CD8^+$ T cells. Scale bars are 100 μm.

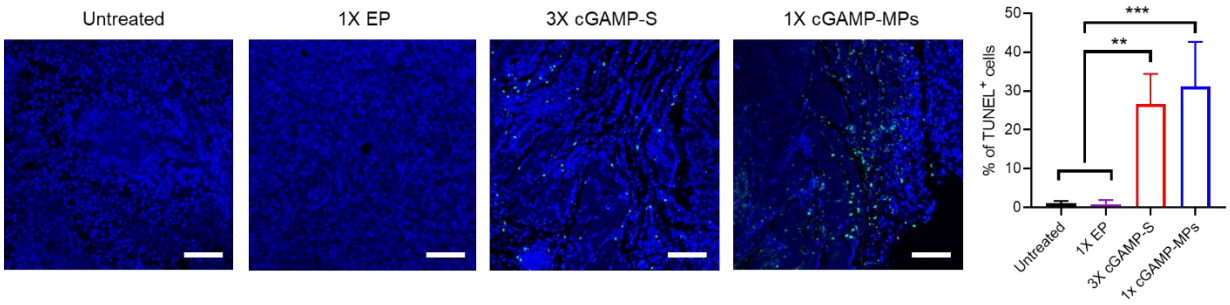

Fig. S15. TUNEL staining of histological sections of B16F10 tumors after treatments. Blue represents DAPI staining of nuclei. Green represents apoptotic cells stained by TUNEL assay kit. Scale bars are 100 μm. Data are shown as mean ± SD (n = 4). Statistical significance was calculated by one-way ANOVA. **P < 0.01, ***P < 0.001.

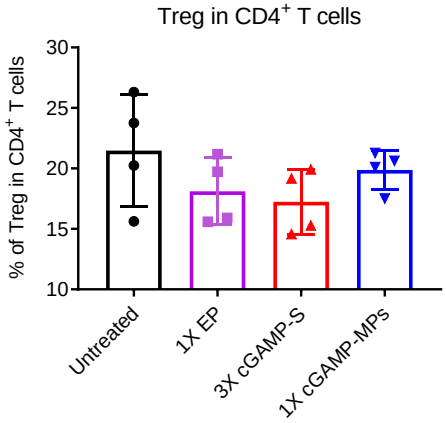

Fig. S16. Analysis of regulatory T cells in the TME after treatments. Data are shown as mean ± SD (n = 4). There were no statistical differences between groups. Statistical significance was calculated by one-way ANOVA.

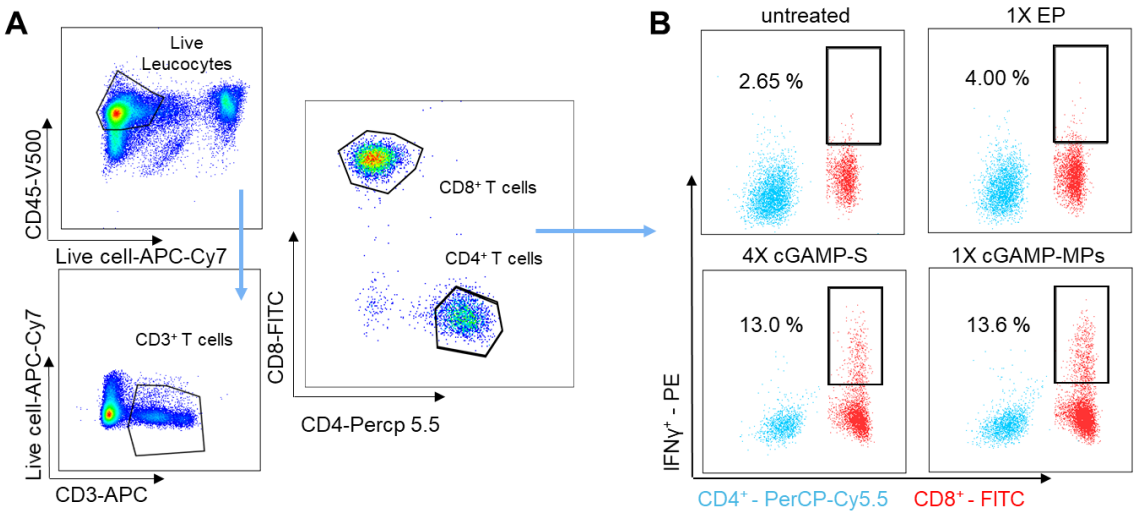

Fig. S17. Flow cytometry measurements of T cells in systemic circulation. A. Gating scheme for flow cytometry measurements of $CD4^+$ and $CD8^+$ T cells in systemic circulation. **B.** Scatter plots of $IFN\gamma^+CD8^+$ and $IFN\gamma^+CD4^+$ T cells in the serum collected 21 days after tumor inoculation (treatment scheme was shown in Fig. 3D).

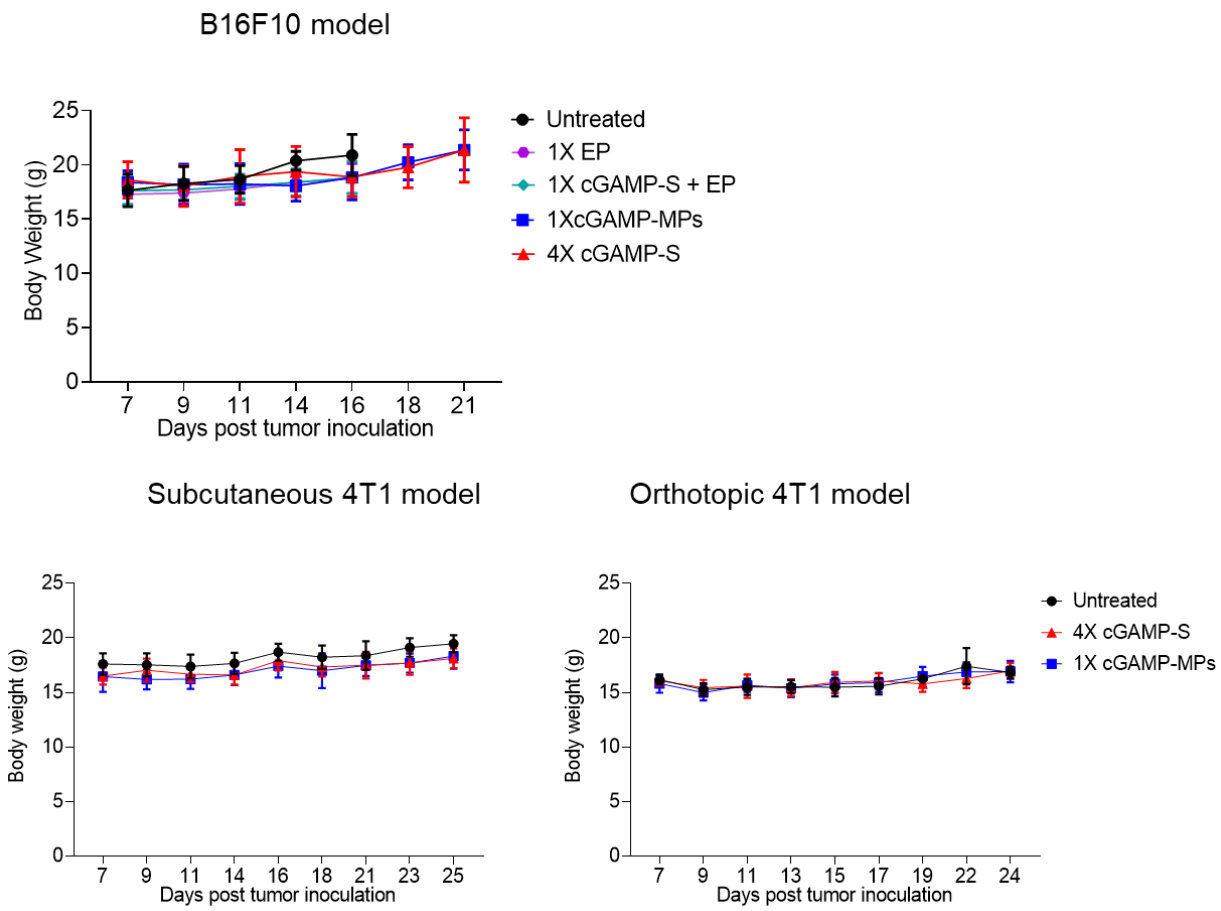

Fig. S18. Body weight analysis of mice bearing B16F10 melanoma and 4T1 breast tumors after treatments. See Fig. 3D for treatment regimen. Data are shown as mean ± SD (n = 8).

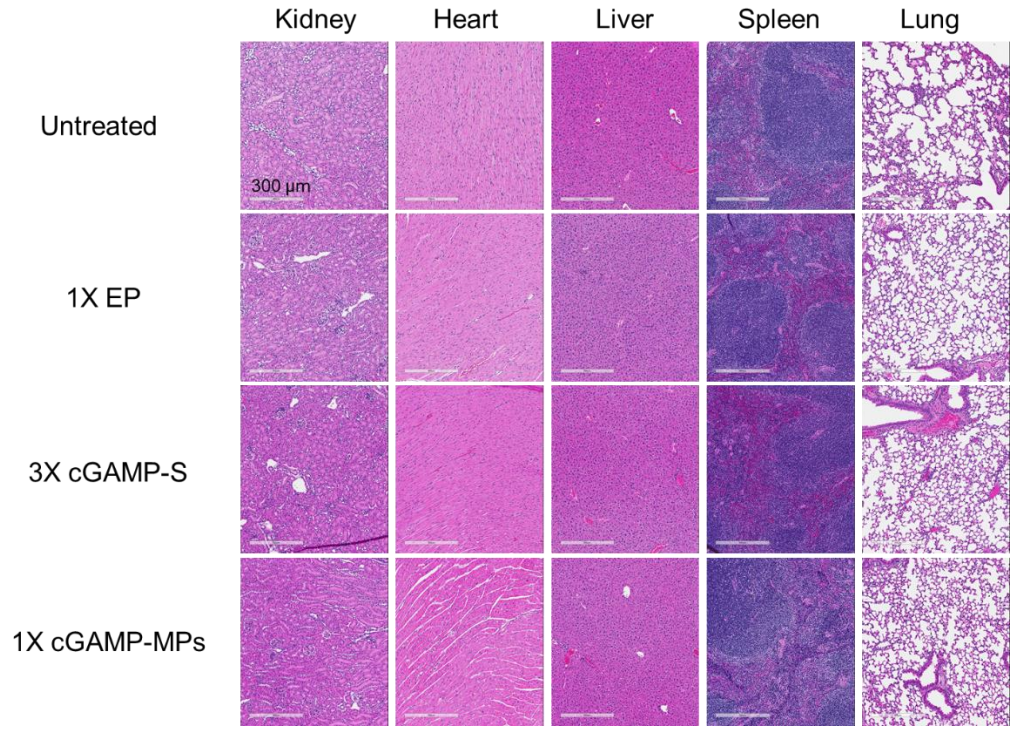

Fig. S19. H&E-stained sections of major organs from B16F10 tumor–bearing mice after different treatments. Scale bars are 300 μm.

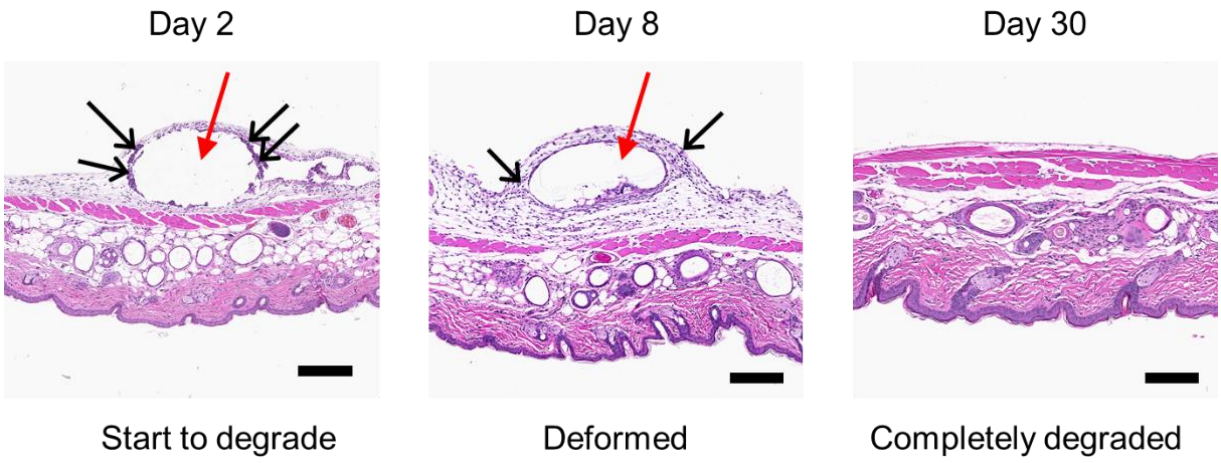

Fig. S20. H&E staining images showing PLGA microparticles deformed and completely degraded over time in vivo. Representative microscopic images of H&E stained skin tissue from immunocompetent hairless mice at day 2, 8, and 30 after subcutaneous injection of PLGA-2 particles. Red arrows point to the location of PLGA-2. Black arrows point to lymphocytes and leucocytes. Scale bars are 200 µm.

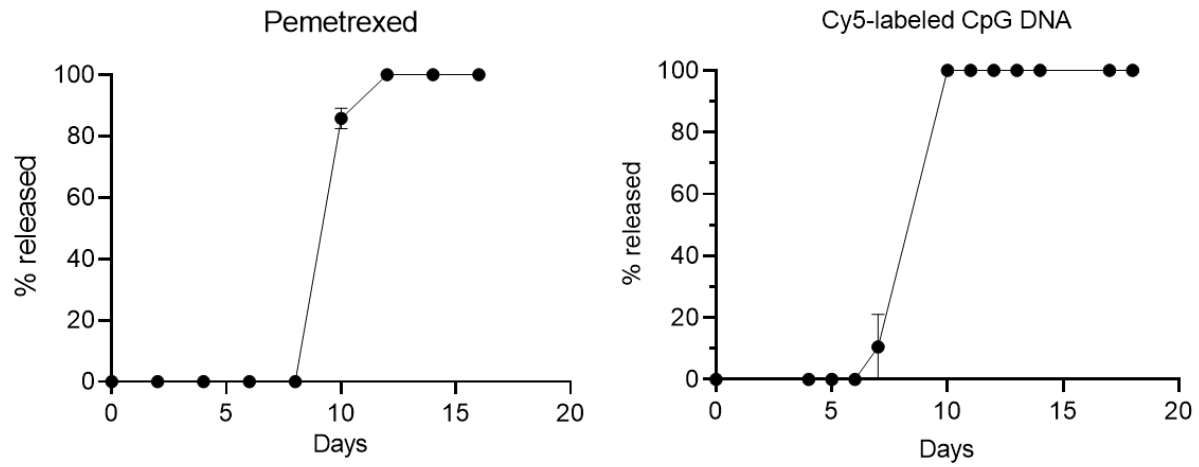

Fig. S21. Cumulative in vitro release kinetics of pemetrexed- and Cy5-labeled CpG DNA from PLGA-2. Data are shown as mean ± SEM (n = 6 to 10).

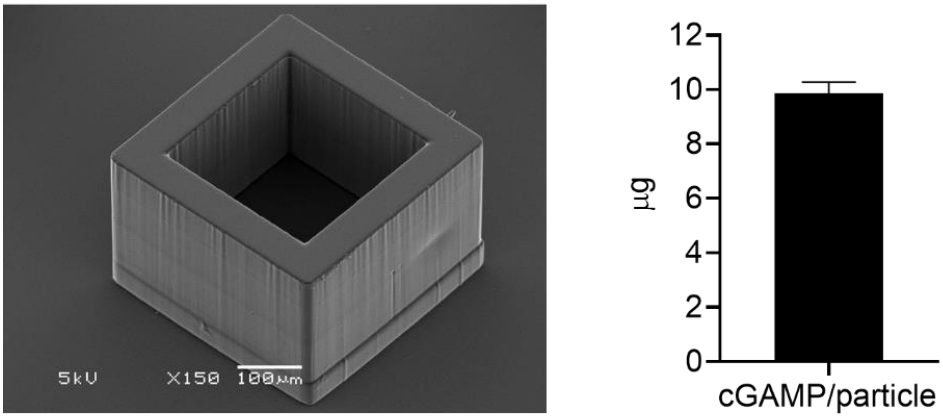

Fig. S22. Representative scanning electron microscopy image of a thinner-walled microparticle and cGAMP loading per particle. The outer dimensions of the particle were 400 × 400 × 300 µm (length × width × height), and wall thickness was 50 µm in each dimension. Data are shown as mean ± SD (n = 4).

Table S1. PLGA compositions and in vitro release time points of AF647-dextran from different PLGA-MPs. The molecular weight of PLGA was measured by tetrahydrofuran gel permeation chromatography with a light scattering detector. Data are shown as mean ± SD (n = 6 to 8). M_n, M_w, and PDI represent number averaged molecular weight, weight averaged molecular weight, and polydispersity index, respectively.

Name	M_n (kDa)	M_w (kDa)	PDI	Chain end	Lactide: glycolide ratio	Release time (days)
PLGA-1	4.4	8.4	1.91	acid	50:50	4±0
PLGA-2	9.1	16.6	1.83	acid	50:50	8±0
PLGA-3	12.1	22.2	1.83	acid	60:40	11±1
PLGA-4	3.7	6.1	1.64	acid	50:50	1±0
PLGA-5	28.9	49.5	1.71	acid	50:50	15±1
PLGA-6	7.6	13.4	1.75	ester	50:50	18±1
PLGA-7	71.5	121.2	1.82	ester	75:25	97±2